JGR Oceans

RESEARCH ARTICLE
10.1029/2020JC016654

Direct and Indirect Pathways of Convected Water Masses and Their impacts on the Overturning Dynamics of the Labrador Sea

Sotiria Georgiou[1], Stefanie L. Ypma[1,2], Nils Brüggemann[3], Juan-Manuel Sayol[1,4], Carine G. van der Boog[1], Paul Spence[5], Julie D. Pietrzak[1], and Caroline A. Katsman[1]

[1]Section of Environmental Fluid Mechanics, Faculty of Civil Engineering and Geosciences, Delft University of Technology, Delft, The Netherlands, [2]Institute for Marine and Atmospheric Research Utrecht, Utrecht University, Utrecht, Netherlands, [3]Faculty of Mathematics, Informatics and Natural Sciences, University of Hamburg, Hamburg, Germany, [4]Department of Applied Mathematics, University of Alicante, Sant Vicent del Raspeig, Alicante, Spain, [5]School of Geosciences, University of Sydney, Sydney, NSW, Australia

Key Points:

- Convected waters follow either a fast direct route or a slow indirect route regulated by local eddy activity before exiting the Labrador Sea
- Argo float trajectories confirm these direct and indirect routes, which typically display a 2.5-year difference in Labrador Sea Water (LSW) export timescales
- As both routes add to the overturning in the basin, our study implies complex links between variability in LSW formation and the Atlantic Meridional Overturning Circulation

Supporting Information:

- Supporting information S1

Correspondence to:
S. Georgiou,
S.Georgiou@tudelft.nl

Citation:
Georgiou, S., Ypma, S. L., Brüggemann, N., Sayol, J-M., van der Boog, C. G., Spence, P., et al. (2021). Direct and indirect pathways of convected water masses and their impacts on the overturning dynamics of the Labrador Sea. *Journal of Geophysical Research: Oceans*, *126*, e2020JC016654. https://doi.org/10.1029/2020JC016654

Received 28 JUL 2020
Accepted 18 NOV 2020

Abstract The dense waters formed by wintertime convection in the Labrador Sea play a key role in setting the properties of the deep Atlantic Ocean. To understand how variability in their production might affect the Atlantic Meridional Overturning Circulation (AMOC) variability, it is essential to determine pathways and associated timescales of their export. In this study, we analyze the trajectories of Argo floats and of Lagrangian particles launched at 53°N in the boundary current and traced backward in time in a high-resolution model, to identify and quantify the importance of upstream pathways. We find that 85% of the transport carried by the particles at 53°N originates from Cape Farewell, and it is split between a direct route that follows the boundary current and an indirect route involving boundary-interior exchanges. Although both routes contribute roughly equally to the maximum overturning, the indirect route governs its signal in denser layers. This indirect route has two branches: part of the convected water is exported rapidly on the Labrador side of the basin and part follows a longer route toward Greenland and is then carried with the boundary current. Export timescales of these two branches typically differ by 2.5 years. This study thus shows that boundary-interior exchanges are important for the pathways and the properties of water masses arriving at 53°N. It reveals a complex three-dimensional view of the convected water export, with implications for the arrival time of signals of variability therein at 53°N and thus for our understanding of the AMOC.

Plain Language Summary In the North Atlantic Ocean, due to the local atmospheric conditions, lighter waters originating from the subtropics transform to denser waters that flow southwards in deeper layers in a circulation pattern known as the Atlantic Meridional Overturning Circulation (AMOC). This transformation occurs, among others, in the Labrador Sea and its strength and the properties of the transformed water vary from year to year. Knowledge of how the transformed water spreads from the basin through the global ocean is needed to understand how any variability in its signal may affect the AMOC's strength. We investigate the pathways that water masses follow in a reference frame that moves along with the flow. We find that 85% of the transport at 53°N follows either a fast, direct route from Cape Farewell via the boundary current, or a slower, indirect route between these locations that involves boundary-interior exchanges. These exchanges govern the export routes of the transformed water, its properties and the arrival time of its signature at 53°N. This implies that a better understanding of the processes that control export along these routes and the variability therein is needed to interpret link between water mass transformation in the Labrador Sea and AMOC variability.

1. Introduction

The subpolar North Atlantic (SPNA) is a region of high importance for the global climate (e.g., Buckley & Marshall, 2016; Lozier et al., 2019; Schott & Brandt, 2007) and in particular for the Atlantic Meridional Overturning Circulation (AMOC). There, the conversion of the relatively warm and salty waters flowing northward in the North Atlantic Current (NAC, upper AMOC limb) to cold and slightly fresher North Atlantic Deep Water (NADW, lower AMOC limb) takes place. The NADW is a combination of the Labrador

Sea Water (LSW) and the dense overflow waters originating from the Nordic Seas (Talley et al., 2011). During wintertime, the heat loss from the ocean to the atmosphere together with the weak stratification below the mixed layer facilitates the process of convection at certain locations in the SPNA. Traditionally, the LSW was considered the product of deep convection that takes place in the central Labrador Sea (Marshall & Schott, 1999; Talley & McCartney, 1982). However, more recent studies revealed that deep convection also occurs in the southern Irminger Sea and that this results in a water mass with similar properties similar to LSW (de Jong et al., 2012; Le Bras et al., 2020; Pickart et al., 2003; Piron et al., 2016; Våge et al., 2008).

Previous numerical model studies suggested a strong connection between LSW production and AMOC variability (e.g., Biastoch et al., 2008; Kuhlbrodt et al., 2007; Rahmstorf et al., 2015). However, recent observational studies have cast doubts on the importance of LSW production for the AMOC and pointed out a stronger connection with water mass transformation in the eastern part of the SPNA instead (Li & Lozier, 2018; Lozier et al., 2019; Zou et al., 2020). Consequently, the connection between the LSW production and the variability of the AMOC is under renewed debate.

One of the key elements in understanding a potential connection between LSW formation and the AMOC is to clarify the relative importance of all possible export pathways of LSW and the associated timescales. Although the processes that govern the conversion of lighter to denser water masses and the locations where this occurs have been extensively researched in numerical and observational studies (e.g Marshall & Schott, 1999; Pickart & Spall, 2007; Spall & Pickart, 2001; Våge et al., 2008), the processes that govern the export routes of dense water masses are less well understood.

LSW pathways are the subject of numerous observational and numerical studies (e.g., Bower et al., 2009; Brandt et al., 2007; Palter et al., 2008; Rhein et al., 2017; Straneo et al., 2003; Talley & McCartney, 1982) and the fact that multiple pathways have been identified illustrates the complex nature of the LSW spreading. The LSW mainly follows the Deep Western Boundary Current (DWBC) and spreads equatorward along the western boundary of the North Atlantic (Handmann et al., 2018; Le Bras et al., 2017; Stramma et al., 2004; Talley & McCartney, 1982). At the transition between the SPNA and the subtropics, the presence of significant exchange between the DWBC and the interior causes the DWBC to bifurcate from its equatorward flow, thus resulting in interior pathways of LSW in the SPNA (e.g., Bower et al., 2009; Solodoch et al., 2020; Spence et al., 2012). The main pathways that newly formed LSW follows prior to entering the DWBC have also been identified. Within the Labrador Sea itself, LSW may be rapidly exported by spreading laterally near the Labrador coast, directly formed in the boundary current as a result of convection within the boundary current itself (e.g., Brandt et al., 2007), or first travel from the interior toward the west coast of Greenland and then follow the boundary current (e.g., Georgiou et al., 2020; Palter et al., 2008). Moreover, the LSW may travel northeastward toward the Irminger Sea (e.g., Bower et al., 2009; Pickart et al., 2003), possibly carried by mid-depth recirculation cells (e.g., Lavender et al., 2000).

However, the processes that govern the transport along these various export routes of dense water masses formed in the Labrador Sea have yet to be clarified; in particular, quantification of the magnitude of the transports, the typical water mass properties, and travel times associated with each pathway are still lacking. It is expected that the arrival of a LSW signal at the locations of the OSNAP array (north of 52°N; Lozier et al., 2019) and RAPID-MOCHA array (at 26.5°N; Smeed et al., 2018) will differ depending on the pathway that LSW follows. The recent idealized study of Georgiou et al. (2020) indicates that this is indeed the case, but the idealizations did not allow for a reliable quantification of timescales. This complexity clearly makes it difficult to capture a potential link between formation rates of dense waters and AMOC variability further downstream.

In this study, we analyze the upstream pathways of all water masses exiting the Labrador Sea at 53°N revealed by Lagrangian particle tracking, using the model output from a state-of-the-art global ocean-sea ice model. Our approach and analyses strongly build on the highly idealized model study of Georgiou et al. (2020) in which qualitative insights gained. The use of output from a realistic simulation introduces among others more realistic atmospheric forcing, more realistic bathymetry, the effects of salinity, potential connections between the sub-basins of the SPNA and the presence of overflow waters and allows us to characterize the transports and water mass transformation along pathways quantitatively. In addition, we

analyze the trajectories of available Argo floats to identify pathways and associated time scales of deeper water masses within the Labrador Sea from observations.

The Argo float data, the global ocean-sea ice model simulation, and the Lagrangian particle tracking approach are introduced in Section 2. The upstream pathways of the water masses found at 53°N from the Argo float trajectories and the trajectories from the high-resolution model are analyzed in Section 3. The subduction location of the particles, the properties they consequently acquire and the pathways that follow after being subducted are explored in Section 4. In Section 4, we also investigate the relative importance of each pathway on the overturning in the Labrador Sea. Furthermore, the travel times of particles along the various pathways are addressed in Section 5. Finally, a discussion on the three-dimensional view of the export of convected waters is provided in Section 6, followed by the summary and conclusions of our results (Section 7).

2. Data and Methods

To establish the possible upstream pathways for LSW within the subpolar gyre, we first use the trajectories derived from available Argo floats (Section 2.1). The limited number and lifetime of the Argo floats prohibit the quantification of transports along each of these pathways. In addition, their isobaric drift does not allow the investigation of the water mass transformation occurring along the various pathways or the vertical displacement of the water masses. Therefore, a Lagrangian study using the output of a realistic global ocean model is performed. The model data and the Lagrangian approach are introduced in Sections 2.2 and 2.3.

2.1. Argo Float Data

The data used in this study are obtained from the International Argo Program (downloaded on May 15, 2020 from https://coriolis.eu.org, Argo, 2020). The floats are designed to drift at approximate pressures of 1,000, 1,500 or 2,000 db for 10 days. Then, each float descends to 2,000 db and collects profiles of the water column as it rises to the surface where it remains only shortly to communicate with the Argos satellite system (Roemmich et al., 2009). Once the float has transmitted its data, it descends again to its designated drifting depth. The Argo float then repeats this cycle, usually with a 10-day period. We select only those floats that at some moment are found in the subpolar gyre and exit the Labrador Sea via the boundary current at 53°N and onshore of the 3,000 m isobath. This procedures selects 97 floats; all trajectories are mapped in Figure 1a and are analyzed further in Section 3.1.

2.2. Ocean Circulation Model: MOM

We use the output data from the Modular Ocean Model (MOM) global ocean-sea ice model, to advect the Lagrangian particles. For a more detailed description of its configuration, we refer to Spence et al. (2017). MOM uses a tripolar B-grid with a horizontal resolution of 0.1° (which corresponds to ∼ 5.5 km at 60°N) and 50 vertical layers with a resolution of 5 m at the surface up to 200 m near the bottom. The model is forced with 6-hourly COREv2-NYF (Griffies et al., 2009; Large & Yeager, 2009) atmospheric forcing and the associated bulk formulations, in particular the Normal Year Forcing derived from the interannual varying atmospheric state from 1958 to 2000. Moreover, the model is coupled to the GFDL Sea Ice Simulator model, which allows the sea ice to freely evolve. In addition, a restoring condition with a timescale of 60 days is applied to the surface salinity.

Vertical mixing (and in particular the process of convection) is parameterized by the KPP parameterization (Large et al., 1994), while biharmonic viscosity and diffusion are applied in the horizontal. The ratio of the baroclinic radius of deformation to a model's grid spacing is commonly used as a measure for the ability of the model to resolve the mesoscale activity (Hallberg, 2013). Within the SPNA the Rossby radius is ∼ 10 km (Funk et al., 2009; Smith et al., 2000), thus the horizontal resolution of MOM is only partly eddy-resolving in this region.

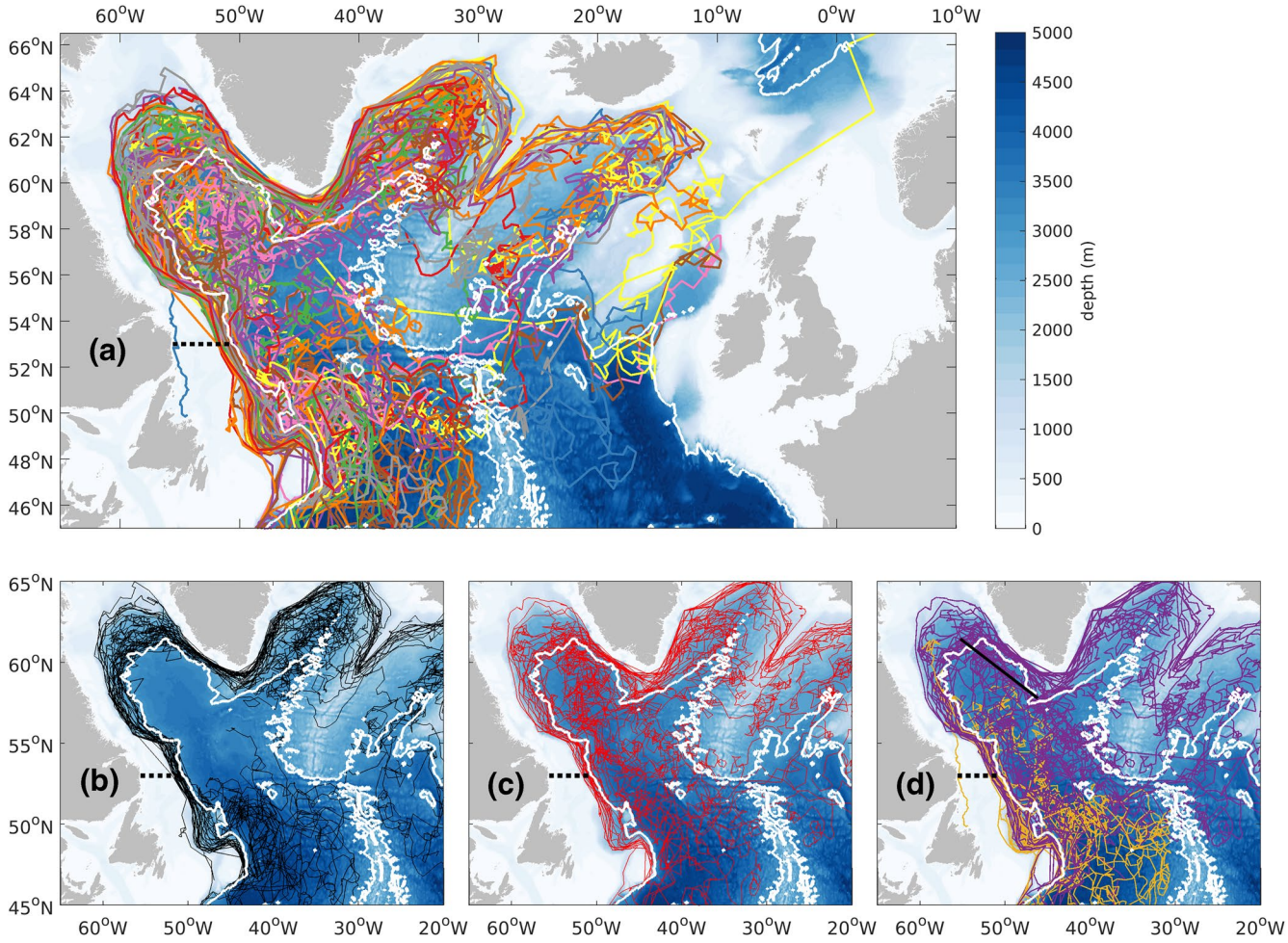

Figure 1. (a) Trajectories of 97 Argo floats that drift in the subpolar gyre and exit the Labrador Sea via the boundary current (onshore of the 3,000 m isobath at 53°N, black dotted line). (b) and (c) Example trajectories of floats that (b) drift within the boundary current (ARGO-BC, always onshore of the 3,000 m isobath, 32 floats), (c) enter the interior of the Labrador Sea (ARGO-interior, 65 floats). (d) Subset of the float trajectories in (c), distinguishing between floats that are laterally advected directly from the interior to exit the Labrador Sea (ARGO-LC, trajectories in yellow, 16 floats) or reveal an exchange between the interior and the boundary current near the West Greenland coast (ARGO-WG, trajectories in purple, 49 floats). The line used to separate the ARGO-WG and ARGO-LC floats is shown in black in (d). The 3,000 m isobath is highlighted (white contour, bathymetry data from ETOPO1; Amante & Eakins, 2009).

Ypma et al. (2019) found that this MOM simulation generally shows a good agreement with the observed hydrography in the Nordic Seas. Here, we shortly discuss the hydrography, the mixed layer depth and eddy kinetic energy in the SPNA Ocean derived from the annual mean three-dimensional velocity, potential temperature, and salinity fields. The analysis is performed on model data obtained following a 70-year-long control state simulation in this high resolution.

Following Talley and McCartney (1982), we define LSW as the water mass for which the potential vorticity (PV) is PV $< 4 \times 10^{-12}$ m^{-1} s^{-1}, which in this MOM simulation corresponds to the density range $\sigma = 27.75$–27.83 kg m^{-3}. The overflow water is defined as $\sigma > 27.83$ kg m^{-3} (Figure S1b–S1c). The densities of LSW and overflow waters thus display a small positive bias compared to densities typically assigned to LSW ($\sigma = 27.70$–27.80 kg m^{-3}) and overflow water ($\sigma > 27.80$ kg m^{-3}) in observational studies (e.g., Holliday et al., 2018). Such small biases in the simulated hydrography of the Labrador Sea in the MOM simulation are comparable to what is seen in other high-resolution modelling studies (e.g., Zou & Lozier, 2016). In the presented analysis, we identify LSW based on this density range deduced from the model.

To characterize the main currents in the SPNA, we first calculate the depth-integrated transports, and next assess the cumulative transport from the Labrador coast toward Scotland. We use the local minima and

maxima of this cumulative transport to define the horizontal extent of each current (marked by orange vertical lines in Figure S1d). The corresponding transport for each major current obtained in this way (Table S1) compares well to the observed values (Holliday et al., 2018). Moreover, we calculated the overturning in density space as from the MOM data along the approximate OSNAP section, following the methodology described in Zou et al. (2020) (Figure S1e). The modeled overturning strength compares well to the observed values, both over the full section and along the OSNAP-WEST and OSNAP-EAST sections (Table S2).

The location and the depth of convection are analyzed from the winter (January-March, JFM) mean mixed layer depth (MLD_{JFM}), defined from a density difference criterion: an increase of $\Delta\sigma = 0.01$ kg m^{-3} with respect to the surface value (Brandt et al., 2007; MacGilchrist et al., 2020; Paquin et al., 2016). In MOM, convection reaches a depth of 1,400 m in the central Labrador Sea (Figure S2a). The largest values are found in the southwest, away from the locations where the heat loss (black contour in Figure S2a) and mesoscale eddy activity (shading in Figure S2b) peak. Overall, the location and the depth of the convection region in the Labrador Sea agree well with observations (Pickart et al., 2002; Våge et al., 2009). The surface eddy kinetic energy (EKE, Figure S2b) displays maximum values near the West Greenland continental slope and reduces offshore in a tongue-like pattern similarly to studies that derive EKE from altimetry (e.g., Lilly et al., 2003; Prater, 2002).

To summarize, the hydrography and currents simulated in MOM represent the observations well, which makes it a suitable tool for our study. In particular, the representation of the deep convection, the properties of the water masses and the key features of the eddy field are in good agreement with observations.

2.3. Lagrangian Particle Tracking

To investigate the possible upstream pathways and the origins of the water masses that exit the Labrador Sea via the western boundary current, numerical particles are released along a zonal transect at 53°N extending from the coast until the 3,000 m isobath (dotted line in Figure 2) and advected backward in time using the Connectivity Modeling System (CMS, Paris et al., 2013). We selected to release the Lagrangian particles at 53°N because it is a location that is commonly thought as the exit of the Labrador Sea, but also because it is a region where recurrent measurements of the DWBC take place (e.g., Fischer et al., 2010). In addition, releasing particles south of 53°N (around Flemish Cap) would need a longer simulation time to account for the interior pathways discussed in Section 1 (Bower et al., 2009; Solodoch et al., 2020; Spence et al., 2012). The particles are advected for 6 years using the 5-day mean three-dimensional velocity field of MOM. Since a normal year-forcing is applied to MOM, year-to-year variability in velocities is expected to be small. Therefore, we use only one year of model data that is representative of its Eulerian mean state and repeat this as input for CMS for simplicity.

The particles are released at a resolution of 0.1° in longitude and 50 m in the vertical, only when the meridional velocity is southward at these locations. A volume transport is assigned to each particle, defined by multiplying the meridional velocity in the grid box in which the particle is released by the area of the grid box (Döös, 1995). The transport carried by each particle remains constant throughout its trajectory (van Sebille et al., 2018). Particles are released daily, for a period of 1 year. All transport calculations are done by adding the volume transport carried by all particles divided by the number of release days. In total, 839,002 particles are launched, representing a total annual mean transport of 25.3 Sv.

The particles are advected with a timestep of 1 h within the three-dimensional velocity field of MOM. CMS uses a tricubic interpolation and a fourth-order Runge Kutta stepping scheme to calculate the new position of each particle in space and time, respectively. The vertical movements associated with the process of convection are parameterized in CMS: when particles are in the mixed layer, a random contribution is added to the vertical velocity with a maximum speed of $|w| = 10$ cm s^{-1} (van Sebille et al., 2013; Ypma et al., 2019) to mimic the strong non-hydrostatic vertical motions associated with small-scale convective plumes (Marshall & Schott, 1999).

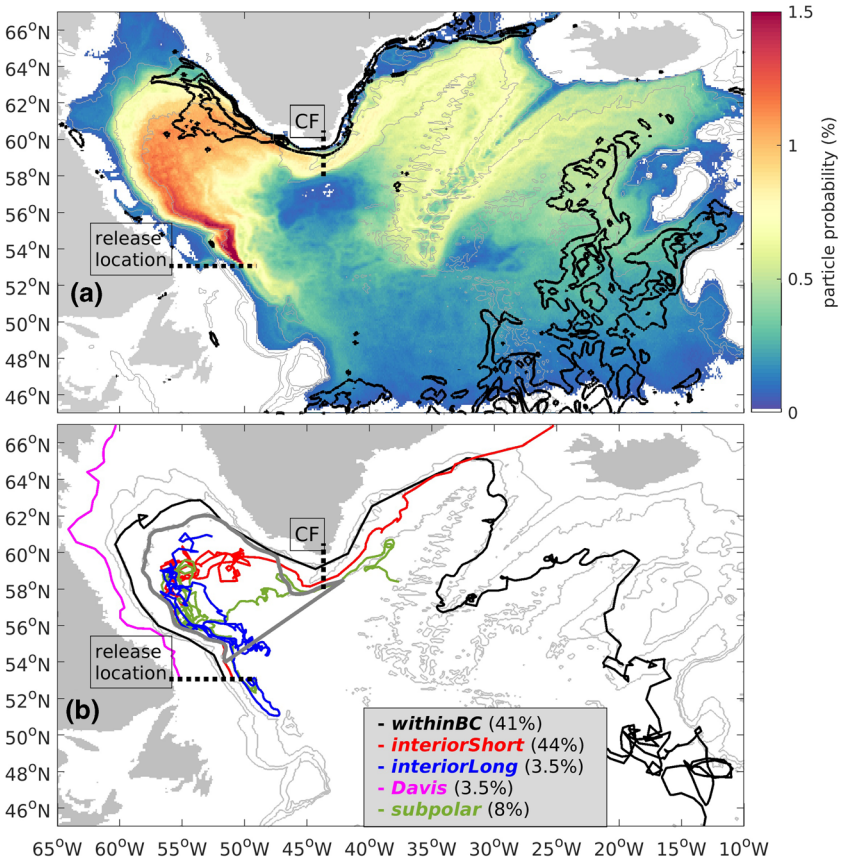

Figure 2. (a) Particle probability map (shading) highlighting the main pathways of waters upstream of the release location (dotted black line at 53°N). Black contours indicate the annual mean EKE (contour interval is 200 $cm^2\ s^{-2}$, starting from the contour line of 200 $cm^2\ s^{-2}$). (b) Five example trajectories of particles categorized and color-coded depending on their pathways; *subpolar* particle (green trajectory), *interiorShort* particle (red trajectory), *withinBC* particle (black trajectory), *interiorLong* particle (blue trajectory) and *Davis* particle (magenta trajectory). The section at 44°W (CF) and the 3,000 m isobath (dark gray contour) are used to separate the particles (see text for details on the procedure). Numbers in the legend indicate the percentage of the total transport carried by each pathway. CF, Cape Farewell.

3. Pathways Upstream of 53°N

We first analyze the pathways of water masses found in the boundary current at 53°N, both from the float data (Section 3.1) and from the Lagrangian analysis (Section 3.2).

3.1. Pathways from Argo Float Data

The float trajectories clearly reveal pathways involving exchanges between the boundary current and the interior of the Labrador Sea (Figure 1a). To distinguish if a float is in the interior or in the boundary current, we use the 3,000 m isobath. To filter out possible short excursions of floats into the interior, we require that a float is found in the interior for more than 10 subsequent cycles (see Section 2.1) to be labeled as being in the interior. We find 32 floats that continuously drift within the boundary current (ARGO-BC, Figure 1b) and 65 floats that are in the interior at some time before they exit the Labrador Sea with a southward direction at 53°N (ARGO-interior, Figure 1c). It appears that some of these ARGO-interior floats travel directly from the interior to the Labrador Current on the western side of the basin while others follow more complex pathways: they first travel toward the West Greenland coast and then follow the boundary current to exit the basin. To be able to separate the floats based on these two types of pathways, we define a boundary in the northeast of the basin (black line in Figure 1d), placed such that it crosses the region of enhanced EKE

known from altimetry data (e.g., Lilly et al., 2003). ARGO-interior floats that reach a position north of this line, that is, those floats that approach the West Greenland (WG) coast after residing in the Labrador Sea interior, are categorized as ARGO-WG (purple trajectories in Figure 1d); the others, which head for the Labrador Current (LC), are labeled as ARGO-LC (yellow trajectories in Figure 1d). Based on this definition, the 65 ARGO-interior floats can be separated in 16 ARGO-LC floats and 49 ARGO-WG floats. Example trajectories of five ARGO-LC and ARGO-WG floats are shown in Figure S3.

The behavior of the ARGO-WG floats supports the view presented in Georgiou et al. (2020) that substantial exchange exists between the boundary current and the interior, and in particular in the eddy-rich region adjacent to the West Greenland coast. In Georgiou et al. (2020), it was shown that the water masses that have been transformed in the interior of the Labrador Sea are transported toward the region of high EKE on the Greenland side by eddy stirring and are then entrained in the boundary current, thus following an indirect route to leave the basin. Although the trajectories of the Argo floats may be affected by the surface currents during the brief period they spend at the surface, it is striking to see that many floats move from the interior toward the boundary along this same indirect route. If their trajectory is mainly governed by flows at their parking depths, which coincides with a depth typical for LSW in the interior (e.g., Bower et al., 2019), this suggests that this indirect LSW export route exists in reality. Moreover, the irregularity of the trajectories in Figure 1d corroborates the view that the presence of the local eddy field steers the pathway of LSW toward the West Greenland coast (Brüggemann & Katsman, 2019; Georgiou et al., 2019, 2020).

3.2. Pathways in MOM

Tracing the Lagrangian particles backward in time allows us to identify the origin of the water masses found in the boundary current at 53°N from the model perspective, and to investigate the main pathways they follow prior to reaching that latitude. A map of the particle probability (Figure 2a) reveals these preferred routes. To construct such a map, following Ypma et al. (2019), we first regrid every particle's positions on a regular $0.1° \times 0.1°$ grid and sum the transport carried through each of these grid boxes, by the particles. Next, this accumulated transport per grid box is divided by the total transport carried by all particles combined (in this case 25.3 Sv, see Section 2.3).

Figure 2a shows that particles seeded at 53°N follow pathways within the boundary current system in the SPNA but also follow pathways through the central Labrador Sea. Moreover, the enhanced particle probability in the vicinity of the west coast of Greenland where the EKE peaks (black contours in Figure 2a) suggests that the local eddy activity plays an important role for directing these pathways between the boundary current and the central Labrador Sea (hereinafter, central-LS), which is in agreement with the idealized model study by Georgiou et al. (2020).

To assess whether similar processes are acting in a realistic model and to quantify the relative importance of the pathways along the perimeter and through the basin interior, we follow a similar approach as in Georgiou et al. (2020) and separate particle pathways by determining if they remain in the boundary current or enter the central-LS.

Within the 6 year advection time, 85% of the particles seeded at 53°N (i.e., 727,066 particles) are traced backward in time to 44°W near Cape Farewell (CF, dotted black line in Figure 2). We subdivide these particles further depending on whether they enter the central-LS between these two sections or not. We define a particle as in the central-LS when it is at least 50 km offshore of the smoothed 3,000 m isobath (dark gray contour in Figure 2b) for more than 20 days, to filter out possible short and fast excursions of particles into the central-LS and back. This results in the definition of three categories (now considering forward in time): particles that enter the Labrador Sea at 44°W offshore of the 3,000 m isobath (hereinafter, *subpolar* particles, green trajectory in Figure 2b), and particles that enter the Labrador Sea at 44°W onshore of the 3,000 m isobath and either cross this isobath into the central-LS at some location (*interiorShort* particles, red example trajectory) or never leave the boundary current (*withinBC* particles, black example trajectory).

Not all the particles launched at 53°N reach 44°W when traced backward in time. It appears that 10% of the particles do enter the central-LS but remain west of CF during the entire 6 year simulation. These particles are referred to as *interiorLong* particles (blue example trajectory in Figure 2b). The remaining 5% of the

particles originate north of 65°N (Davis Strait) and are referred to as *Davis* particles (magenta example trajectory in Figure 2b). The transport carried by the *subpolar*, *interiorShort*, *withinBC*, *interiorLong*, and *Davis* particles amounts to 1.9 Sv, 11.2 Sv, 10.4 Sv, 0.9 Sv, and 0.9 Sv, respectively.

Clearly, the *withinBC* and *interiorShort* particles represent the dominant upstream pathways since together they account for 85% of the total transport arriving at 53°N (22.6 Sv) and this transport is divided roughly equally over these two pathways. We therefore focus on these two particle categories in the remainder of the paper, where we study the transformation of the water masses along these two pathways and their importance for the overturning in the Labrador Sea.

4. Water Mass Transformation in the Labrador Sea

To investigate where in the Labrador Sea the water masses traced by the *withinBC* and *interiorShort* particles change their thermohaline properties, we identify where these particles subduct from the mixed layer, and compare their *T*–*S* properties. Moreover, we investigate the overturning resulting from the water mass transformation occurring along these two pathways (Section 4.1). Furthermore, we track the pathways that the *interiorShort* particles follow after subduction and explore their final properties at 53°N (Section 4.2).

4.1. Subduction of Water Masses and Resulting Overturning

We calculate the local subduction velocity as the sum of the transports of all particles that subduct within a certain grid box divided by its area, again using a regular 0.1° × 0.1° grid (Brandt et al., 2007; Georgiou et al., 2020). The subduction velocity for the *withinBC* particles (Figure 3a) peaks in the western part of the Labrador Sea. This subduction region was also identified in Brandt et al. (2007), Palter et al. (2008), Georgiou et al. (2020), and MacGilchrist et al. (2020) and reflects convection that takes place in the boundary current itself. In addition, enhanced subduction velocities are found in a narrow strip along CF. The total subduction rate of the *withinBC* particles in the Labrador Sea amounts to 2.4 Sv. For the *interiorShort* particles, high subduction velocities are found mainly in the central-LS and in the southwest of the basin (Figure 3b). The total subduction of the *interiorShort* particles amounts to 6.4 Sv of which 4.8 Sv occurs in the central-LS (i.e., offshore of the gray contour line in Figure 3b) and 1.6 Sv in the boundary current. Thus, in our analysis, 46% of the total subduction in the Labrador Sea occurs along the boundary current and 54% in the interior of the basin. In a recent study, MacGilchrist et al. (2020) performed a Lagrangian analysis of the subduction of NADW only, by tracking its pathways backward from the deep North Atlantic. They also note a prominent role for subduction in the boundary current. According to this study, 60% of the total NADW ventilation results from subduction within the boundary current and about 25% from subduction in the interior of the Labrador Sea. It is yet unclear how to interpret this difference, as the applied model, the particle seeding strategy and water masses analyzed all differ from our analysis. The fact that most of the *interiorShort* particles subduct in the central-LS and then re-enter the boundary current prior to exiting the basin corroborates the importance of exchanges between the boundary current and the central-LS in regulating the properties of the water masses arriving at 53°N.

Figures 3c and 3d, a *T*–*S* diagram of particle probability showing the temperature and salinity for the *withinBC* and *interiorShort* particles, show that the subduction location of the particles and their final properties at 53°N are linked. The thermohaline properties of the *withinBC* and *interiorShort* particles that subduct in the Labrador Sea clearly differ; *withinBC* particles are relatively light, with densities σ_{53^oN} = 27.55–27.79 kg m^{-3} (Figure 3c), while *interiorShort* particles are denser with σ_{53^oN} = 27.62–27.83 kg m^{-3} (Figure 3d). Notably, *withinBC* particles that subduct near CF (delineated by the dashed contour in Figure 3c) are lighter (σ = 27.55–27.63 kg m^{-3}) than particles that subduct elsewhere in the boundary current (σ = 27.63–27.79 kg m^{-3}). This is in agreement with the idealized studies by Spall (2004), Straneo (2006), and Brüggemann and Katsman (2019) that all showed that the boundary current gets denser in downstream direction due to buoyancy loss that it experiences.

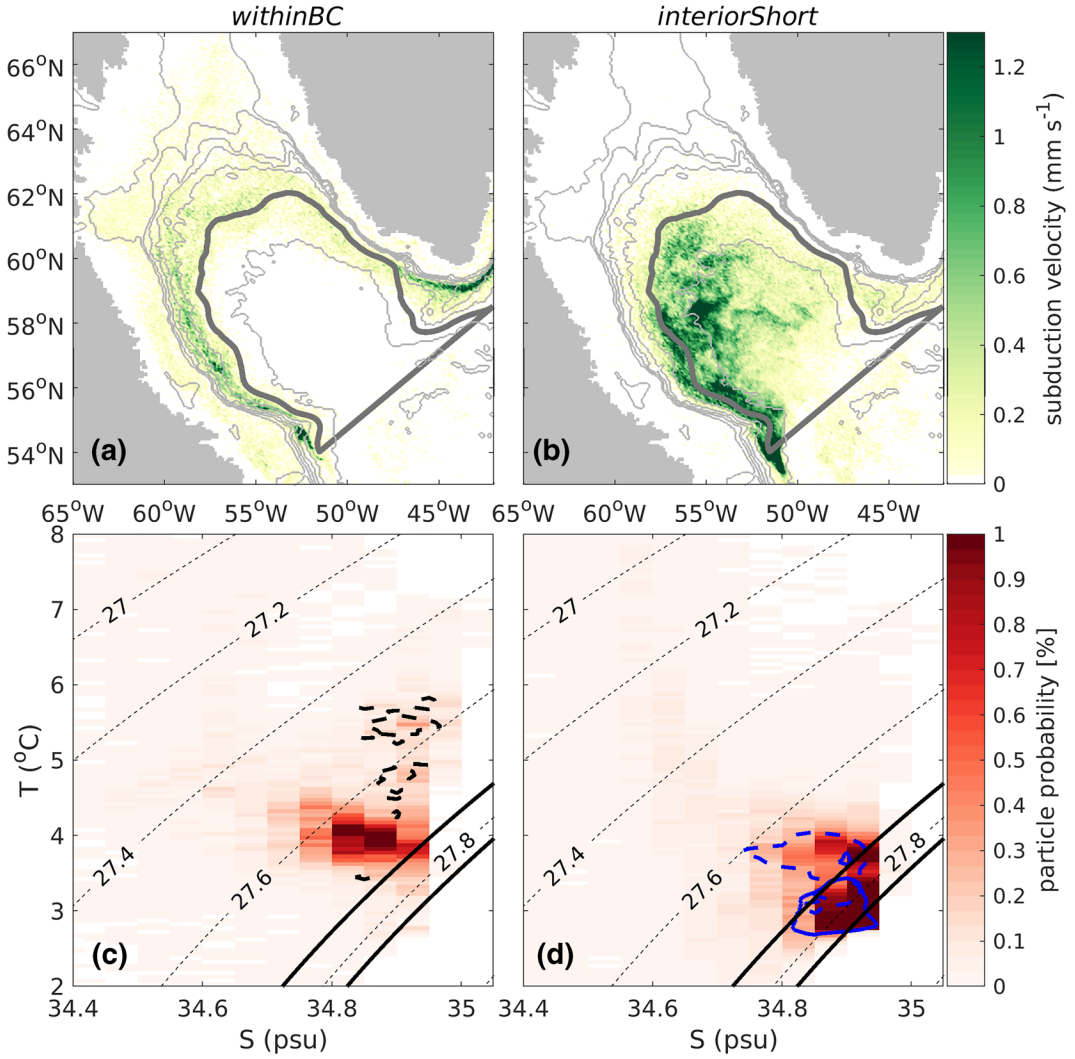

Figure 3. (a) and (b) Mean subduction velocity for (a) *withinBC* and (b) *interiorShort* particles. The 3,000 m isobath used to distinguish the boundary current from the central-LS is indicated by the dark gray contour line. (c) and (d) *T*–*S* diagram of the thermohaline properties of the (c) *withinBC* and (d) *interiorShort* particles at 53°N in terms of particle probability. The latter is calculated as the sum of the transports associated with all particles in a certain ΔT–ΔS bin divided by the total transport carried by the associated pathway (Ypma et al., 2019). The black dotted lines outline the isopycnals (in kg m^{-3}); thick black lines indicate the LSW density range in MOM. The black dashed contour in (c) encompasses 70% of the *withinBC* particles that subduct south of Greenland; the blue dashed (solid) contour in (d) encompasses 70% of the *interiorShort* particles that subduct in the boundary current (central-LS).

For the *interiorShort* particles, two clear peaks can be distinguished in the *T*–*S* diagram. Particles that subduct within the boundary current in the southwest (encompassed by the dashed contour in Figure 3d) are lighter than particles that subduct in the central-LS (solid contour in Figure 3d), with densities σ_{53^oN} = 27.60–27.80 kg m^{-3} and σ_{53^oN} = 27.73–27.83 kg m^{-3}, respectively. This is a result of the stronger buoyancy loss over the central-LS, yielding a denser product of convection.

Both the subducted *withinBC* and *interiorShort* consist of water masses with densities within the density range of the LSW in this model (thick black lines in Figures 3c and 3d). However, we found that less than 5% of the total subduction of the *withinBC* particles is associated with the LSW density range compared to 43% of the total subduction of the *interiorShort* particles. That is, our results indicate that the transformation of the *withinBC* particles, which only follow the boundary current, results into relatively lighter water masses

than the transformation of the *interiorShort* particles. Note that the subduction of the *interiorShort* particles may occur both in the central-LS and in the boundary current.

We evaluated the overturning in the Labrador Sea resulting from this water mass transformation (see supporting information for details on the method) solely based on the transports carried by the *withinBC* and *interiorShort* particles. The overturning based on these two classes of particles peaks at $\sigma = 27.60$ kg m^{-3} and amounts to 4.3 Sv (purple line in Figure S4a). In temperature and salinity space, we find a maximum overturning of 9.1 Sv and 9.7 Sv at 4.2 °C and 34.94 psu, respectively (Figure S4b–S4c and Table S3), indicating that substantial density compensation occurs (Zou et al., 2020).

The *withinBC* and *interiorShort* pathways contribute roughly equally to the net Lagrangian overturning in the Labrador Sea. The maximum overturning resulting from the *withinBC* particles (black lines in Figure S4) occurs at a lighter density (higher temperature) than the overturning resulting from the *interiorShort* particles (red lines) at $\sigma = 27.60$ kg m^{-3} and $\sigma = 27.65$ kg m^{-3} (4.4 and 3.7 °C), respectively. Interestingly, the overturning associated with the *interiorShort* particles shows significant contributions in the density range $\sigma = 27.75$–27.82 kg m^{-3}, which is within the signature of the LSW in this model (Section 2.2); the overturning associated with the *withinBC* particles is negligible at this density range. This once more confirms that the denser water masses are formed in the central-LS, whereas convection along the boundary current results in lighter water masses. The fact that the signal of the various direct and indirect pathways of water masses is evident in the overturning signal within different density classes emphasizes the complex nature of processes regulating the overturning in the Labrador Sea.

4.2. Pathways and Final Properties of Convected Water Masses

The *T*–*S* diagrams in Figures 3c and 3d reveal that the densest water masses that exit the Labrador Sea at 53°N are associated with the *interiorShort* particles that subduct in the central-LS. So, we now further investigate the pathways and properties of this subset of *interiorShort* particles, which represent 4.8 Sv (75%) of the 6.4 Sv of subduction that takes place in the Labrador Sea. Visual inspection of their trajectories reveal two preferred routes from their subduction location to 53°N: particles tend to either travel toward the west coast of Greenland or toward the Labrador side of the basin before re-entering the boundary current.

This is in agreement with the idealized studies of Brüggemann and Katsman (2019) and Georgiou et al. (2020) who showed by using passive tracers that the densest water masses formed in the interior of the basin are steered toward the topographic narrowing aided by the velocity shear induced by the presence of the eddy field. In particular, Brüggemann and Katsman (2019) showed that convected waters formed in the basin interior move along isopycnals from the convection region toward the boundary current in the east, and mainly toward the topographic narrowing. This process can be thought of as a stochastic path of particles influenced by the eddies: in regions where a lot of eddies are present, the particles are steered in all directions. When a particle then enters a region of low eddy activity, it will move much slower and might be considered "stuck" in such a relatively quiet region. However, if a particle remains in the region of high EKE, the eddies can advect it further, in any direction. Following these arguments, the particles will be distributed everywhere within the high EKE region and will eventually also reach the West Greenland coast. That is, the limited extent of the EKE field yields a particle pathway mimicking a random walk with a preferred direction.

Therefore, we further separate the subset of *interiorShort* particles based on their proximity to the high EKE region near Greenland (Figures 4a and 4b). Analogous to the analysis of the Argo floats presented in Section 3.1, we define a boundary in the northeast (black line in Figures 4a and 4b), placed such that EKE < 200 cm^2 s^{-2} southwest of it. Particles that at some time cross this line from southwest to northeast are classified as following the WG path; all other particles are considered to follow the LC-path. It appears that most newly formed dense water leaves the central-LS following the direct LC path (3.0 Sv; 60% of the total transport of this subset of particles), but that the indirect WG-path also contributes significantly (1.8 Sv; 40%).

Example trajectories for these two pathways are shown in Figures 4a and 4b, traveling from their subduction location (magenta dots) to 53°N. To better visualize preferred routes Figures 4c and 4d shows maps

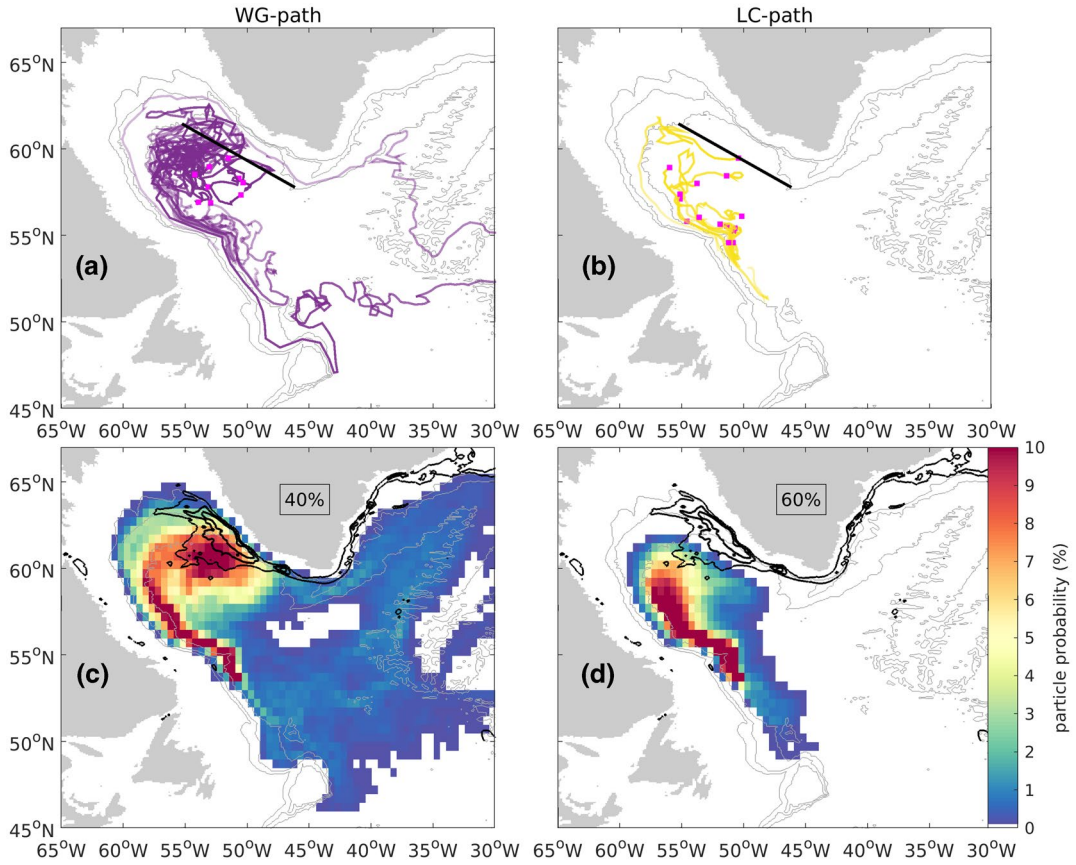

Figure 4. (a) and (b) Example trajectories for the subset of *interiorShort* particles that subduct in the central-LS, from their subduction location (magenta dots) to 53°N and (c) and (d) associated particle probability map. The set of particles is split by evaluating if they (a) and (c) travel toward the west coast of Greenland (WG-path) by crossing the black line in (a) and (b) or (b) and (d) travel toward the Labrador coast (LC-path). Northeast of the black line in (a) and (b) the EKE is higher than 200 $cm^2\ s^{-2}$; black contours in (c) and (d) indicate the annual mean EKE (contour interval is 200 $cm^2\ s^{-2}$, starting from the contour line of 200 $cm^2\ s^{-2}$). Also shown in (c) and (d) is the percentage of the volume transport carried by the WG-LC paths with respect to the total carried by this subset of the *interiorShort* particles. EKE, eddy kinetic energy.

of the particle probability for these two pathways (maps are constructed as Figure 2a). For the WG-path (Figure 4c), the particle probability is significantly high at the west coast of Greenland and is co-located with the region of enhanced EKE (black contours), indicating that the WG-path is regulated by the local eddy activity since eddies are needed to steer the dense waters into the boundary current (Brüggemann & Katsman, 2019). Particles that follow the WG-path are steered toward Greenland and then flow cyclonically around the basin to 53°N, yielding a peak in particle probability at the Labrador side (Figure 4c). The particle probability for the LC-path (Figure 4d) outlines the direct export route of newly formed water masses from the central-LS to the boundary current at the Labrador side (Brandt et al., 2007; Georgiou et al., 2020; Palter et al., 2008).

To investigate the water mass properties of this subset of the *interiorShort* particles that subduct in the central-LS when exiting the Labrador Sea, we analyze their transport per density bin at 53°N (Figures 5a and 5b). For the WG- and LC-paths, the maximum transport at 53°N is found at a density range of σ = 27.81–27.82 kg m^{-3}, which corresponds to the denser limit of the LSW density range in this model (see Section 2.2). Interestingly, 30% of the transport carried by the WG-path particles is found within this LSW density range compared to 15% of the transport carried by the LC-path particles. Clearly, relatively light waters are carried mostly along the LC-path. This corroborates that the denser water masses formed in the central-LS most likely follow the indirect route described by the WG-path. The vertical distribution of the particle transport

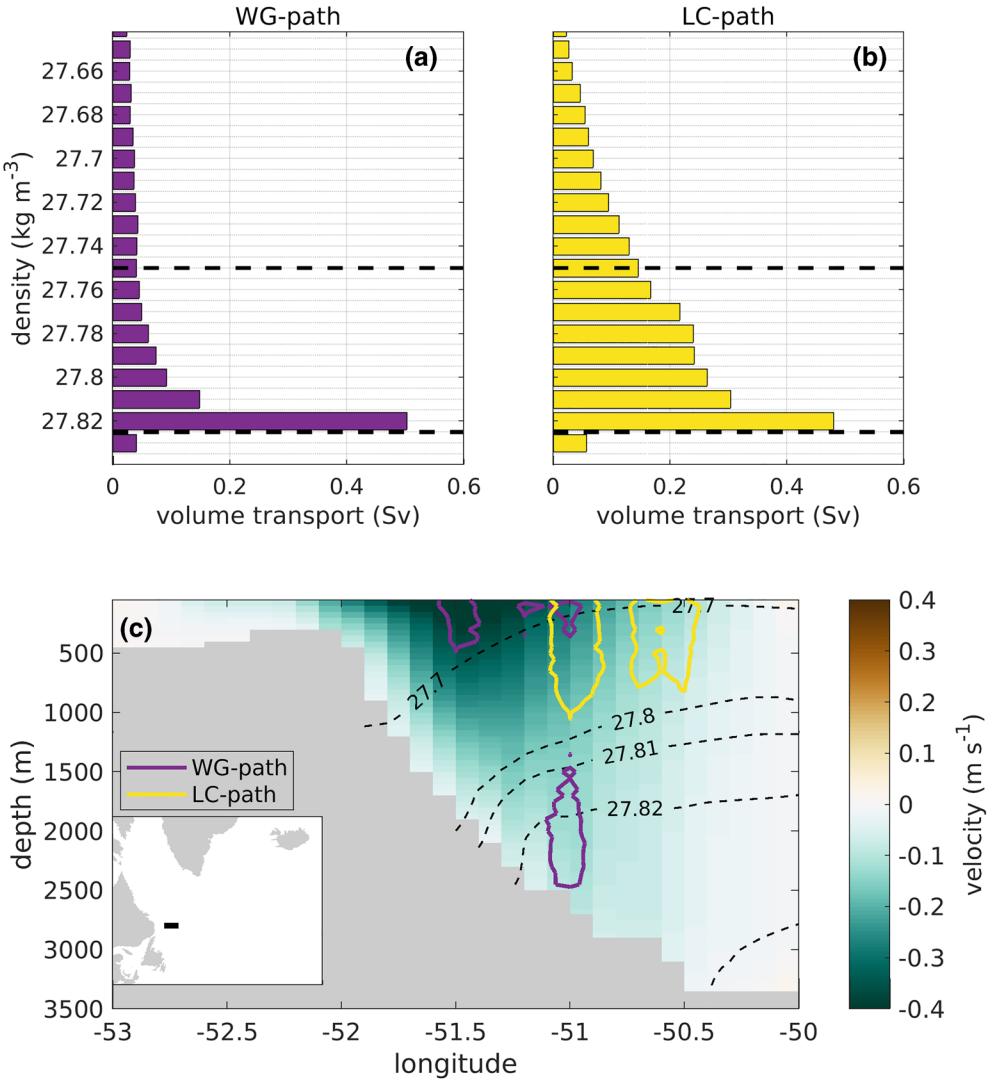

Figure 5. (a) and (b) Volume transport at 53°N carried by the particles that subducted in the central-LS and then travel toward (a) the vicinity of the west coast of Greenland (WG-path) and (b) the Labrador side (LC-path) binned by 0.01 kg m^{-3} in density space. Black dashed horizontal lines in (a)-(b) indicate the LSW density range in MOM. (c) Cross section of the vertical distribution of the volume transport associated with the two pathways at 53°N (black line in the inset): WG-path (purple contours) and LC-path (yellow contours) together with the annual mean velocity of the simulation (shading). Purple (yellow) contours encompass 60% of the WG-path (LC-path) particles. The dashed contours outline the isopycnals (in kg m^{-3}). LSW, Labrador Sea Water; MOM, Modular Ocean Model.

when they reach 53°N (Figure 5c) also reflects that the WG-path carries the denser water masses, since these particles are found deeper in the water column than the particles that follow the LC-path (Figure 5c).

In summary, we have shown in this section that water mass transformation occurs along each of the main pathways (i.e. *withinBC* and *interiorShort*), resulting in water masses with different thermohaline properties. As the pathways that waters follow after subduction are linked to different density classes, clearly this regulates the overturning in the Labrador Sea. Moreover, an export pathway of LSW exists that approaches the West Greenland coast, like the pathway found in Georgiou et al. (2020). The transport carried via this WG-path is about half of that carried along the LC-path, thus implying that the presence of eddies plays a crucial role in shaping the pathways of the convected water (Brüggemann & Katsman, 2019).

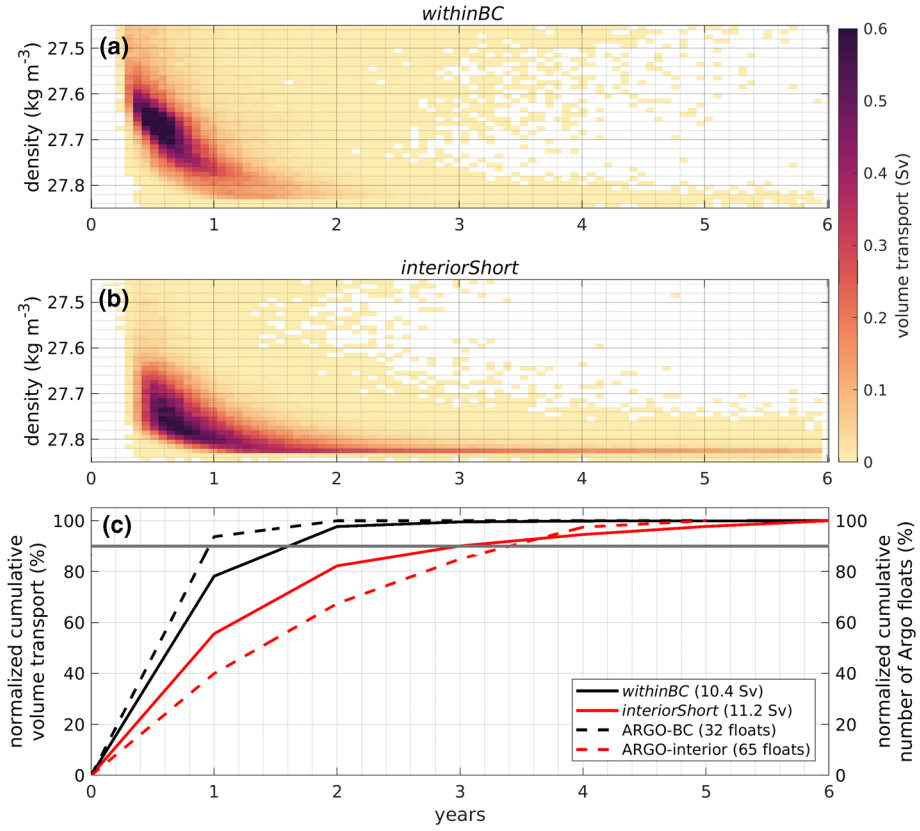

Figure 6. Volume transport carried by the particles as a function of residence time and density at 53°N (σ_{53^oN} in kg m^{-3}) for the (a) *withinBC* and (b) *interiorShort* particles. The volume transport is binned in $\Delta\sigma = 0.01$ kg m^{-3} and $\Delta t = 25$ day intervals. (c) Normalized cumulative volume transport of the *withinBC* (black line) and *interiorShort* (red line) particles and normalized cumulative number of Argo floats that either travel within the boundary current (ARGO-BC, black dashed line) or are found in the central-LS at some moment (ARGO-interior, red dashed line), as a function of residence time. Gray horizontal line in (c) indicates the 90% limit. Float trajectories for ARGO-BC and ARGO-interior are shown in Figures 1b and 1c, respectively.

5. Timescales Associated with the Pathways

It is expected that the various pathways that particles follow prior to exiting the Labrador Sea at 53°N affect the associated timescales: the residence time of water masses in the Labrador Sea and the time from subduction to arrival at 53°N.

First, we focus on their residence time in the Labrador Sea: the time it takes for a particle to travel from CF (dotted line in Figure 2b) to 53°N, and how this depends on a particle's density at 53°N which in turn reflects the water mass transformation it experienced in the basin (Section 4).

The *withinBC* particles are characterized by a short residence time (Figure 6a); almost all particles reach 53°N in less than 2 years. From these particles, the ones that represent lighter water masses (density range of σ_{53^oN} = 27.60–27.70 kg m^{-3}) arrive 53°N within 5–8 months; their transport amounts to 3.9 Sv. The *withinBC* particles with $\sigma_{53^oN} > 27.75$ kg m^{-3}, which represent a smaller transport (2.1 Sv), display longer residence times between 6 months and 2 years. The *interiorShort* particles associated with relatively light water masses (i.e., density range σ_{53^oN} = 27.65–27.75 kg m^{-3}) are relatively fast, with a residence time of less than a year (Figure 6b) and their transport amounts to 3.2 Sv. However, the majority of the *interiorShort* particles (7.3 Sv) have longer residence times, up to the 6 years maximum advection time (Figure 6b). They are associated with the LSW density range in MOM (i.e., σ = 27.75–27.83 kg m^{-3}). This confirms the

findings from the idealized study of Georgiou et al. (2020), that the densest water masses formed in the interior of the Labrador Sea stay in the basin longer.

We also estimate the residence time of the Argo floats (Sections 2.1 and 3.1) for comparison. Since their starting locations differ, we now define the residence time as the time it takes to travel from the location where they are first found in the Labrador Sea until they reach 53°N. As for the particles, we distinguish the floats that travel in the boundary current the entire time (ARGO-BC floats, $n = 32$, see Figure 1b) from those that at some moment are located in the central-LS (ARGO-interior floats, $n = 65$). It is clear from Figure 6c that the ARGO-BC floats (dashed black line) reach 53°N faster than the ARGO-interior floats (dashed red line): 90% of the ARGO-BC floats arrives within 1 year; for the ARGO-interior floats this takes 3.5 years. The estimated residence times for the floats correspond well to the results obtained from the Lagrangian particles: 90% of the transport carried by the *withinBC* and *interiorShort* particles reaches 53°N within 1.5 and 3 years, respectively (black and red solid lines in Figure 6c). The results are in agreement with the timescales reported in observational (Palter et al., 2008) and modeling (Brandt et al., 2007) studies.

Next, we investigate the impacts of the pathways (and hence of the boundary-interior exchange) for the export timescales of the particles that subduct in the central-LS, distinguishing the WG- and LC-paths as in Section 4. The export timescale is defined as the time it takes a particle to travel from its final subduction location to 53°N. It is found that the water masses that follow the LC-path (i.e. toward the Labrador side) are rapidly exported from the Labrador Sea; 90% of the transport carried by the LC-path is exported within 15 months (not shown). This is in agreement with previous studies that showed that the newly formed LSW is rapidly exported from the interior of the basin by being entrained in the boundary current (e.g., Brandt et al., 2007; Georgiou et al., 2020). Not surprisingly, the export timescales of water masses that follow the indirect WG-path are much longer; 90% of the transport carried by the WG-path is exported within 4 years (not shown).

The finding that the transport of convected water from the interior toward the west coast of Greenland takes almost 2.5 years longer than the direct transport on the Labrador side, combined with the fact that different water masses are formed along these pathways, has important implications for the variability in transport of these water masses to be expected downstream in response to variations in LSW formation rates.

6. A Three-Dimensional View on the Export of Convected Waters

In this study, we showed that the different pathways that water masses follow in the Labrador Sea follow prior to reaching at 53°N (Figure 2b) have a direct impact on the water mass properties with which they arrive there and on their residence time in the basin, and hence on the Labrador Sea overturning dynamics.

The analysis of the pathways of the water masses that are transformed in the central-LS (i.e., the WG-LC- paths, Section 4.2), clearly shows that the local eddy activity regulates their fate in the Labrador Sea (Figures 4 and 5). The denser water masses formed in the central-LS tend to follow either a direct route toward the Labrador side (LC-path) or a more complex pathway that seems to be steered by the eddy activity near the west coast of Greenland (WG-path). In the idealized model simulation of Brüggemann and Katsman (2019), the dense water masses that have been formed by convection in the interior are laterally transported toward the boundary current along isopycnals. To investigate if this is also the case in this realistic model, we analyze the re-entry of the particles in the boundary current after subduction in the central-LS. To this end, we investigate where the particles cross the 3,000 m isobath for the last time (our definition of re-entry of the boundary current) and with what density (σ_{crossing}), and compare this to the local annual mean density of the boundary current, $\overline{\sigma}_{3{,}000\,m}$ (Figure 7).

It appears that most WG-path particles re-enter the boundary current at a distance between 800 and 1,100 km downstream from 44°W (purple shading in Figure 7a), which coincides with the region of enhanced EKE. This entrainment occurs between 2,100 and 2,800 m depth where the annual mean density of the boundary current is $\overline{\sigma}_{3{,}000\,m}$ >27.82 kg m^{-3} (contours). In contrast, the majority of the LC-path particles re-enter the boundary current at 2,000–2,150 km downstream from 44°W (Figure 7c) and at shallower depths (500–2,000 m). At this depth and location, the boundary current has a mean density $\overline{\sigma}_{3{,}000\,m} = 27.70$–$27.82$ kg m^{-3}.

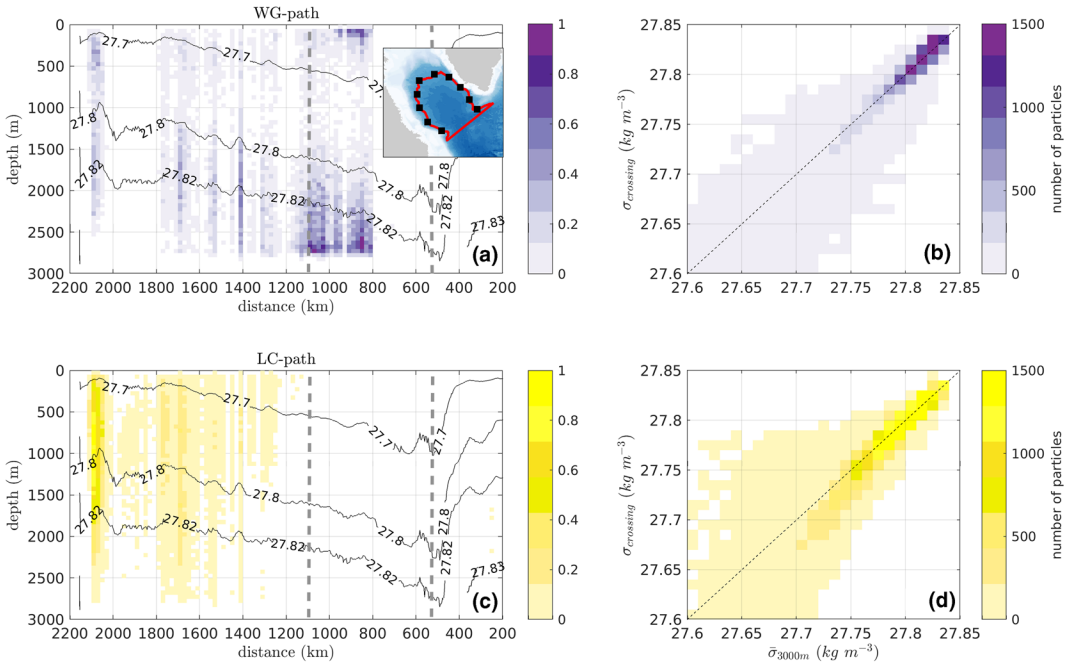

Figure 7. (a) and (c) Normalized number of particles that cross the 3,000 m isobath and re-enter the boundary current as a function of distance downstream of CF and depth, for (a) the WG-path (purple shading) and (c) the LC-path (yellow shading). Particles are binned over segments of 30 m in depth and 50 km in alongshore direction, starting from 44°W (see inset in [a], black squares mark distances of 200 km). Note that the horizontal axis is flipped. The black contours outline the annual mean density of the boundary current as a function ($\bar{\sigma}_{3,000\,m}$, in kg m^{-3}) of the alongshore coordinate. Gray dashed contours denote the region near the WG coast where EKE > 200 cm^2 s^{-2}. (b) and (d) Scatter plot of the density of particles when they cross the 3,000 m isobath (σ_{crossing}, in kg m^{-3}) versus the annual mean density of the boundary current $\bar{\sigma}_{3,000\,m}$ at this location, for particles that follow (b) the WG-path and (d) the LC-path in terms of number of particle. The latter is calculated as the sum of particles in a certain $\Delta\sigma$–$\Delta\sigma$ bin ($\Delta\sigma$ = 0.01 kg m^{-3}). CF, Cape Farewell; LC, Labrador Current; WG, West Greenland.

The density of the particles that re-enter the boundary current by crossing the 3,000 m isobath (σ_{crossing}) is highly correlated to the mean density of the boundary current ($\bar{\sigma}_{3,000\,m}$) at the location of the crossing (Figures 7b and 7d). This supports the view that the entrainment of convected waters in the boundary current occurs along isopycnals (Brüggemann & Katsman, 2019). It also implies that this entrainment can only take place where the density and depth of the convected water mass match the local properties of the boundary current, which adds a potentially strong constraint on this process. This view is in agreement with the result that convected water with of varying density is entrained in the boundary current at the Labrador side (LC-path, Figure 5b), while only the densest convected waters re-enter the boundary current along the WG-path (Figure 5a). Near the Greenland coast, the stronger stratification resulting from the advection of buoyant water from the boundary current by the eddies effectively blocks the re-entry of lighter convected waters ($\sigma \simeq$ 27.70–27.75 kg m^{-3}) there. At the topographic narrowing, the isopycnals are strongly tilted downward in the direction of the coast. This induces an along-isopycnic transport of the densest water masses from the interior toward the boundary current in deeper layers (Brüggemann & Katsman, 2019). As a consequence, at 53°N, the denser water masses that follow the WG-path are found deeper in the water column than those that follow the LC-path (Figure 5c) since they follow different isopycnals in the boundary current (Figure 7a).

7. Summary and Conclusions

In this study, we use Lagrangian particles launched at 53°N and traced backward in time using the output of an ocean eddy-permitting model (MOM) to investigate the upstream pathways of the water masses that exit the Labrador Sea. The motivation of this study stems from the need to improve our understanding on

the export routes of the water masses that constitute the lower limb of the AMOC. In particular, building on the insights gained from the idealized Lagrangian study of Georgiou et al. (2020), we explore the relative importance of the different pathways that water masses follow prior to exiting the Labrador Sea at 53°N by investigating the water mass transformation along these pathways, the impact on the overturning in the basin, and the residence and export timescales associated with the pathways in this more realistic ocean model.

We show that in this model simulation, 85% of the total transport carried by the launched particles follow either the boundary current (*withinBC* particles) or a more complex route that involves boundary current-interior exchanges (*interiorShort* particles) from CF (southern tip of Greenland) to 53°N within a 6 year period (Figure 2). The transformation of the water masses differs along these routes, which leads to differences in their final properties; lighter water masses are formed within the boundary current (*withinBC* particles), while denser water masses are formed in the central-LS (*interiorShort* particles). This is reflected in the relative importance of these pathways for the overturning in density space; the overturning found at densities higher than 27.66 kg m^{-3} is mainly attributed to the *interiorShort* particles (Figure S4a). Only in lighter layers the impact of the transformation of the *withinBC* particles is important. Thus, we conclude that the indirect route which is regulated by boundary current-interior exchanges is important for the representation of the overturning in denser layers.

With regard to volume transport, our results indicate that the contribution of boundary current subduction is as important as that of subduction in the interior of the Labrador Sea (Section 4.1). This is in line with other studies who found that the boundary current subduction plays a key role (Brandt et al., 2007; MacGilchrist et al., 2020) for the ventilation of the water masses in the Labrador Sea. However, our Lagrangian analysis shows that *interiorShort* particles which are subducted close to or within the boundary current can still take a long route through the interior of the Labrador Sea before they finally exit. Thus, care needs to be taken whether particles which are subducted close or within the boundary current are really confined to the boundary current until they exit the Labrador Sea. Moreover, the water masses transformed in the interior are usually denser than those transformed over the boundary current (Figures 3c and 3d). Thus, the densest water masses formed in the Labrador Sea typically take a longer and more complex route compared to the water masses transformed in the boundary current.

Our investigation of the residence time of the major pathways (i.e. *withinBC* and *interiorShort* particles) shows that lighter water masses formed close to or within the boundary current are exported faster than the denser water masses formed in the central-LS (Figure 6), in line with the more qualitative results obtained from the idealized studies of Brüggemann and Katsman (2019) and Georgiou et al. (2020): 90% of the volume transport carried by the *withinBC* and *interiorShort*particles reaches 53°N within 1.5 and 3 years, respectively (Figure 6c). In particular, we show that the denser water masses formed in the central-LS first follow an eddy-driven path toward the West Greenland coast (WG-path, Figure 4a) and re-enter in the boundary current there before reaching 53°N. Therefore, these water masses travel longer distances than the ones that formed within the boundary current itself (*withinBC* particles) or the lighter water masses that formed in the central-LS and are rapidly exported at the Labrador side (LC-path). Last, we showed that the entrainment of convected water mass can only take place where its density and depth match the local properties of the boundary current, which adds a potentially strong constraint on this process (Figure 7).

One of the limitations of the Lagrangian analysis in the idealized study of Georgiou et al. (2020) was the lack of a possible connection between the Labrador and the Irminger Sea, as the model domain was limited to the Labrador Sea only. Interestingly, in this study an indication of a connection between the two basins appears; Figures 4a and 4c) show that some particles that follow the WG-path move toward Greenland and travel farther east than 44°W before they reach 53°N. This would be in agreement with a pathway along the mid-depth recirculation cells found in the SPNA (e.g., Bower et al., 2009; Lavender et al., 2000; Lozier, 2012; Rhein et al., 2015), where newly formed LSW flows toward the eastern SPNA (Figure 4c). In our Lagrangian set-up, the transport carried by these particles only amounts to 0.2 Sv. From this low number, one cannot conclude that this potential pathway between the Labrador and Irminger Seas is not relevant, as the strategy we chose for seeding the Lagrangian particles is not suited to address this question. To investigate this pathway explicitly, a different strategy for the deployment of the particles is required.

Furthermore, we find in agreement with recent studies (Lozier et al., 2019; Zou et al., 2020) that the overturning in density space is stronger in the eastern part of the North Atlantic compared to the Labrador Sea (see Figure S1e). It is important to note that the main findings in these observational studies, namely a weak overturning in density space in the Labrador Sea due to the near-compensation of the overturning in temperature and salinity space, only document the net result of the events that take place in the region. Our study reveals the richness of processes and pathways that give rise to this observed net overturning, characterized by a complex interplay between the convective interior, the boundary current and the eddy field. Using a model forced by Normal Year Forcing simplifies the analysis of the Lagrangian particles but prevents us from analyzing any impacts of the known large interannual variability in the surface forcing (Moore et al., 2012). Therefore, it is by no means clear yet how sensitive the water mass transformation processes and pathways are to for example changes in the surface forcing, and at what timescales a potential response to such changes would become apparent as a signal in the net overturning strength. Hence, an obvious next step is to investigate the response of pathways and water mass transformation to anomalies in forcing conditions, by carefully initializing and tracing Lagrangian particles released in different years, using interannually varying velocity fields rather than looping over a one-year data set as is done here.

The relatively long time it takes for *interiorShort* particles to complete the indirect route to 53°N compared to the direct route followed by the *withinBC* particles, and the outcome that for *interiorShort* particles the export timescales depend on pathway and location of re-entry of the boundary current (Figure 6) indicates that care should be taken when attempting to directly relate variability in LSW production to LSW propagation to the subtropics and thus to AMOC variability. This study reveals a complex three-dimensional view of the LSW export and shows that the interior-boundary current exchanges are crucial for the LSW pathways and export timescales. Better understanding of the processes that control the transports along these various pathways and the variability therein is needed to fully understand the connections between the processes occurring in the Labrador Sea and AMOC variability. According to our study, these pathways are strongly governed by the combination of the density and depth of LSW in the interior and the density structure of the boundary current system along the basin's perimeter.

Data Availability Statement

The ARGO data were collected and made freely available by the International Argo Program and the national programs that contribute to it (http://www.argo.ucsd.edu, http://argo.jcommops.org). The Argo Program is part of the Global Ocean Observing System. The mean fields of MOM and the data of the Lagrangian simulation are archived, open-access, at https://doi.org/10.4121/uuid:9bce7f3b-0bcb-4146-99d7-29b94e7fe8a4.

Acknowledgments
The authors would like to thank two anonymous reviewers whose comments improved this paper. S. Georgiou, S. L. Ypma, and J. -M. Sayol were supported by the Netherlands Organisation for Scientific Research (NWO) via VIDI grant 864.13.011 awarded to C. A. Katsman. N. Brüggemann was funded by the Collaborative Research Centre, TRR 181 "Energy Transfer in Atmosphere and Ocean" funded by the Deutsche Forschungsgemeinschaft (DFG, German Research Foundation, Germany) – Projektnummer 274762653. P. Spence is supported by ARC Future Fellowship FT190100413.

References

Amante, C., & Eakins, B. (2009). ETOPO1 1 Arc-Minute Global Relief Model: Procedures, data sources and analysis. *NOAA Technical Memorandum NESDIS NGDC-24*. National Geophysical Data Center, NOAA. https://doi.org/10.7289/V5C8276M

Argo. (2020). Argo float data and metadata from Global Data Assembly Centre (Argo GDAC). *SEANOE*. https://doi.org/10.17882/42182

Biastoch, A., Böning, C. W., Getzlaff, J., Molines, J.-M., & Madec, G. (2008). Causes of interannual–decadal variability in the meridional overturning circulation of the Midlatitude North Atlantic Ocean. *Journal of Climate*, *21*(24), 6599–6615. https://doi.org/10.1175/2008JCLI2404.1

Bower, A., Lozier, S., Biastoch, A., Drouin, K., Foukal, N., Furey, H., et al. (2019). Lagrangian views of the pathways of the Atlantic meridional overturning circulation. *Journal of Geophysical Research: Oceans*, *124*(0), 5313–5335. https://doi.org/10.1029/2019JC015014

Bower, A., Lozier, M. S., Gary, S. F., & Böning, C. W. (2009). Interior pathways of the North Atlantic meridional overturning circulation. *Nature*, *459*, 243–247. https://doi.org/10.1038/nature07979

Brandt, P., Funk, A., Czeschel, L., Eden, C., & Böning, C. W. (2007). Ventilation and transformation of Labrador Sea water and its rapid export in the deep Labrador Current. *Journal of Physical Oceanography*, *37*(4), 946–961. https://doi.org/10.1175/JPO3044.1

Brüggemann, N., & Katsman, C. A. (2019). Dynamics of downwelling in an eddying marginal sea: Contrasting the Eulerian and the isopycnal perspective. *Journal of Physical Oceanography*, *49*(11), 3017–3035. https://doi.org/10.1175/JPO-D-19-0090.1

Buckley, M. W., & Marshall, J. (2016). Observations, inferences, and mechanisms of the Atlantic Meridional Overturning Circulation: A review. *Reviews of Geophysics*, *54*(1), 5–63. https://doi.org/10.1002/2015RG000493

de Jong, M. F., Van Aken, H. M., Våge, K., & Pickart, R. S. (2012). Convective mixing in the central Irminger Sea: 2002–2010. *Deep-Sea Research Part I: Oceanographic Research Papers*, *63*, 36–51. https://doi.org/10.1016/j.dsr.2012.01.003

Döös, K. (1995). Interocean exchange of water masses. *Journal of Geophysical Research*, *100*(C7), 13499–13514. https://doi.org/10.1029/95JC00337

Fischer, J., Visbeck, M., Zantopp, R., & Nunes, N. (2010). Interannual to decadal variability of outflow from the Labrador Sea. *Geophysical Research Letters*, *37*(24). https://doi.org/10.1029/2010GL045321

Funk, A., Brandt, P., & Fischer, T. (2009). Eddy diffusivities estimated from observations in the Labrador Sea. *Journal of Geophysical Research*, *114*, 1–11. https://doi.org/10.1029/2008JC005098

Georgiou, S., van der Boog, C. G., Brüggemann, N., Ypma, S. L., Pietrzak, J. D., & Katsman, C. A. (2019). On the interplay between downwelling, deep convection and mesoscale eddies in the Labrador Sea. *Ocean Modelling*, *135*, 56–70. https://doi.org/10.1016/j.ocemod.2019.02.004

Georgiou, S., Ypma, S. L., Brüggemann, N., Sayol, J.-M., Pietrzak, J. D., & Katsman, C. A. (2020). Pathways of the water masses exiting the Labrador Sea: The importance of boundary–interior exchanges. *Ocean Modelling*, *150*, 101623. https://doi.org/10.1016/j.ocemod.2020.101623

Griffies, S. M., Biastoch, A., Böning, C., Bryan, F., Danabasoglu, G., Chassignet, E. P., et al. (2009). Coordinated Ocean-ice Reference Experiments (COREs). *Ocean Modelling*, *26*(1), 1–46. https://doi.org/10.1016/j.ocemod.2008.08.007

Hallberg, R. (2013). Using a resolution function to regulate parameterizations of oceanic mesoscale eddy effects. *Ocean Modelling*, *72*, 92–103. https://doi.org/10.1016/j.ocemod.2013.08.007

Handmann, P., Fischer, J., Visbeck, M., Karstensen, J., Biastoch, A., Böning, C., & Patara, L. (2018). The deep western boundary current in the labrador sea from observations and a high-resolution model. *Journal of Geophysical Research*, *123*(4), 2829–2850. https://doi.org/10.1002/2017JC013702

Holliday, N. P., Bacon, S., Cunningham, S. A., Gary, S. F., Karstensen, J., King, B. A., et al. (2018). Subpolar North Atlantic Overturning and gyre-scale circulation in the summers of 2014 and 2016. *Journal of Geophysical Research: Oceans*, *123*(7), 4538–4559. https://doi.org/10.1029/2018JC013841

Kuhlbrodt, T., Griesel, A., Montoya, M., Levermann, A., Hofmann, M., & Rahmstorf, S. (2007). On the driving processes of the Atlantic meridional overturning circulation. *Reviews of Geophysics*, *45*(2). https://doi.org/10.1029/2004RG000166

Large, W., McWilliams, J., & Doney, S. (1994). Oceanic vertical mixing: A review and a model with a nonlocal boundary layer parameterization. *Reviews of Geophysics*, *32*(4), 363–403. https://doi.org/10.1029/94RG01872

Large, W., & Yeager, S. (2009). The global climatology of an interannually varying air–sea flux data set. *Climate Dynamics*, *33*(2), 341–364. https://doi.org/10.1007/s00382-008-0441-3

Lavender, K., Davis, R., & Owens, W. (2000). Mid-depth recirculation observed in the interior Labrador and Irminger seas by direct velocity measurements. *Nature*, *407*(6800), 66–69. https://doi.org/10.1038/35024048

Le Bras, I. A., Straneo, F., Holte, J., de Jong, M. F., & Holliday, N. P. (2020). Rapid export of waters formed by convection near the Irminger sea's western boundary. *Geophysical Research Letters*, *47*(3). https://doi.org/10.1029/2019GL085989

Le Bras, I. A., Yashayaev, I., & Toole, J. M. (2017). Tracking Labrador Sea water property signals along the Deep Western Boundary Current. *Journal of Geophysical Research: Oceans*, *122*(7), 5348–5366. https://doi.org/10.1002/2017JC012921

Lilly, J. M., Rhines, P. B., Schott, F., Lavender, K., Lazier, J., Send, U., & D'Asaro, E. (2003). Observations of the Labrador Sea eddy field. *Progress in Oceanography*, *59*(1), 75–176. https://doi.org/10.1016/j.pocean.2003.08.013

Li, F., & Lozier, M. S. (2018). On the linkage between Labrador Sea water volume and overturning circulation in the Labrador Sea: A case study on proxies. *Journal of Climate*, *31*(13), 5225–5241. https://doi.org/10.1175/JCLI-D-17-0692.1

Lozier, M. S. (2012). Overturning in the North Atlantic. *Annual Review of Marine Science*, *4*(1), 291–315. https://doi.org/10.1146/annurev-marine-120710-100740

Lozier, M. S., Li, F., Bacon, S., Bahr, F., Bower, A. S., Cunningham, S. A., et al. (2019). A sea change in our view of overturning in the subpolar North Atlantic. *Science*, *363*(6426), 516–521. https://doi.org/10.1126/science.aau6592

MacGilchrist, G. A., Johnson, H. L., Marshall, D. P., Lique, C., Thomas, M., Jackson, L. C., & Wood, R. A. (2020). Locations and mechanisms of ocean ventilation in the high-latitude North Atlantic in an eddy-permitting ocean model. *Journal of Climate*, 1–61. https://doi.org/10.1175/JCLI-D-20-0191.1

Marshall, J., & Schott, F. (1999). Open-ocean convection: Observations, theory, and models. *Reviews of Geophysics*, *37*(1), 1–64. https://doi.org/10.1029/98RG02739

Moore, G. W. K., Renfrew, I. A., & Pickart, R. S. (2012). Spatial distribution of airsea heat fluxes over the subpolar North Atlantic Ocean. *Geophysical Research Letters*, *39*(18). https://doi.org/10.1029/2012GL053097

Palter, J. B., Lozier, M. S., & Lavender, K. L. (2008). How does Labrador Sea water enter the Deep Western Boundary Current?. *Journal of Physical Oceanography*, *38*(5), 968–983. https://doi.org/10.1175/2007JPO3807.1

Paquin, J.-P., Lu, Y., Higginson, S., Dupont, F., & Garric, G. (2016). Modelled Variations of Deep Convection in the Irminger Sea during 2003–10. *Journal of Physical Oceanography*, *46*(1), 179–196. https://doi.org/10.1175/JPO-D-15-0078.1

Paris, C. B., Helgers, J., van Sebille, E., & Srinivasan, A. (2013). Connectivity modeling system: A probabilistic modeling tool for the multi-scale tracking of biotic and abiotic variability in the ocean. *Environmental Modelling & Software*, *42*, 47–54. https://doi.org/10.1016/j.envsoft.2012.12.006

Pickart, R. S., & Spall, M. A. (2007). Impact of Labrador Sea Convection on the North Atlantic Meridional overturning circulation. *Journal of Physical Oceanography*, *37*(9), 2207–2227. https://doi.org/10.1175/JPO3178.1

Pickart, R. S., Straneo, F., & Moore, G. (2003). Is Labrador Sea Water formed in the Irminger basin? *Deep Sea Research Part I: Oceanographic Research Papers*, *50*(1), 23–52. https://doi.org/10.1016/S0967-0637(02)00134-6

Pickart, R. S., Torres, D. J., & Clarke, R. A. (2002). Hydrography of the Labrador Sea during active convection. *Journal of Physical Oceanography*, *32*(2), 428–457. https://doi.org/10.1175/1520-0485(2002)032⟨0428:HOTLSD⟩2.0.CO;2

Piron, A., Thierry, V., Mercier, H., & Caniaux, G. (2016). Argo float observations of basin-scale deep convection in the Irminger sea during winter 2011–2012. *Deep Sea Research Part I: Oceanographic Research Papers*, *109*, 76–90. https://doi.org/10.1016/j.dsr.2015.12.012

Prater, M. D. (2002). Eddies in the Labrador Sea as observed by profiling RAFOS floats and remote sensing. *Journal of Physical Oceanography*, *32*(2), 411–427. https://doi.org/10.1175/1520-0485(2002)032⟨0411:EITLSA⟩2.0.CO;2

Rahmstorf, S., Box, J. E., Feulner, G., Mann, M. E., Robinson, A., Rutherford, S., & Schaffernicht, E. J. (2015). Exceptional twentieth-century slowdown in Atlantic ocean overturning circulation. *Nature Climate Change*, *5*(5), 475–480. https://doi.org/10.1038/nclimate2554

Rhein, M., Kieke, D., & Steinfeldt, R. (2015). Advection of North Atlantic Deep Water from the Labrador Sea to the southern hemisphere. *Journal of Geophysical Research: Oceans*, *120*(4), 2471–2487. https://doi.org/10.1002/2014JC010605

Rhein, M., Steinfeldt, R., Kieke, D., Stendardo, I., & Yashayaev, I. (2017). Ventilation variability of Labrador Sea Water and its impact on oxygen and anthropogenic carbon: a review. *Philosophical Transactions of the Royal Society A: Mathematical, Physical and Engineering Sciences*, *375*(2102). https://doi.org/10.1098/rsta.2016.0321

Roemmich, D., Johnson, G. C., Riser, S., Davis, R., Gilson, J., Owens, W. B., et al. (2009). The Argo Program: Observing the global ocean with profiling floats. *Oceanography*, *22*(2), 34–43. https://doi.org/10.5670/oceanog.2009.36

Schott, F. A., & Brandt, P. (2007). Circulation and deep water export of the Subpolar North Atlantic during the 1990's. In J. C. H. SchmittnerChiang & J. C. H. Chiang (Eds.), *Ocean circulation: Mechanisms and impacts—Past and future changes of meridional overturning* (pp. 91–118) American Geophysical Union (AGU). https://doi.org/10.1029/173GM08

Smeed, D. A., Josey, S. A., Beaulieu, C., Johns, W. E., Moat, B. I., Frajka-Williams, E., et al. (2018). The North Atlantic Ocean is in a state of reduced overturning. *Geophysical Research Letters*, *45*(3), 1527–1533. https://doi.org/10.1002/2017GL076350

Smith, R. D., Maltrud, M. E., Bryan, F. O., & Hecht, M. W. (2000). Numerical Simulation of the North Atlantic Ocean at 1/10°. *Journal of Physical Oceanography*, *30*(7), 1532–1561. https://doi.org/10.1175/1520-0485(2000)030⟨1532:NSOTNA⟩2.0.CO;2

Solodoch, A., McWilliams, J. C., Stewart, A. L., Gula, J., & Renault, L. (2020). Why does the Deep Western Boundary Current "Leak" around Flemish cap? *Journal of Physical Oceanography*. https://doi.org/10.1175/JPO-D-1-0247.1

Spall, M. A. (2004). Boundary currents and watermass transformation in marginal seas. *Journal of Physical Oceanography*, *34*(5), 1197–1213. https://doi.org/10.1175/1520-0485(2004)034⟨1197:BCAWTI⟩2.0.CO;2

Spall, M. A., & Pickart, R. S. (2001). Where does dense water sink? A subpolar gyre example. *Journal of Physical Oceanography*, *31*(3), 810–826. https://doi.org/10.1175/1520-0485(2001)031⟨0810:WDDWSA⟩2.0.CO;2

Spence, P., Holmes, R. M., Hogg, A. M., Griffies, S. M., Stewart, K. D., & England, M. H. (2017). Localized rapid warming of West Antarctic subsurface waters by remote winds. *Nature Climate Change*, *7*(8), 595–603. https://doi.org/10.1038/nclimate3335

Spence, P., Saenko, O. A., Sijp, W., & Mathew, E. (2012). The role of bottom pressure torques on the interior pathways of North Atlantic deep water. *Journal of Physical Oceanography*, *42*, 110–125. https://doi.org/10.1175/2011JPO4584.1

Stramma, L., Kieke, D., Rhein, M., Schott, F., Yashayaev, I., & Koltermann, K. P. (2004). Deep water changes at the western boundary of the subpolar North Atlantic during 1996 to 2001. *Deep Sea Research Part I: Oceanographic Research Papers*, *51*(8), 1033–1056. https://doi.org/10.1016/j.dsr.2004.04.001

Straneo, F. (2006). On the Connection between dense water formation, overturning, and poleward heat transport in a convective basin. *Journal of Physical Oceanography*, *36*(9), 1822–1840. https://doi.org/10.1175/JPO2932.1

Straneo, F., Pickart, R. S., & Lavender, K. (2003). Spreading of Labrador Sea water: An advective-diffusive study based on Lagrangian data. *Deep-Sea Research Part I-Oceanographic Research Papers*, *50*(6), 701–719. https://doi.org/10.1016/S0967-0637(03)00057-8

Talley, L. D., & McCartney, M. S. (1982). Distribution and circulation of Labrador Sea water. *Journal of Physical Oceanography*, *12*(11), 1189–1205. https://doi.org/10.1175/1520-0485(1982)012⟨1189:DACOLS⟩2.0.CO;2

Talley, L. D., Pickard, G. L., Emery, W. J., & Swift, J. H. (2011). Chapter 9 – Atlantic Ocean. In L. D. Talley, G. L. Pickard, W. J. Emery, & J. H. Swift (Eds.), *Descriptive physical oceanography* (6th ed., pp. 245–301). Boston, MA: Academic Press. https://doi.org/10.1016/B978-0-7506-4552-2.10009-5

Våge, K., Pickart, R. S., Moore, G. W. K., & Ribergaard, M. H. (2008). Winter mixed layer development in the Central Irminger Sea: The effect of strong, intermittent wind events. *Journal of Physical Oceanography*, *38*(3), 541–565. https://doi.org/10.1175/2007JPO3678.1

Våge, K., Pickart, R. S., Thierry, V., Reverdin, G., Lee, C. M., Petrie, B., et al. (2009). Surprising return of deep convection to the subpolar North Atlantic Ocean in winter 2007–2008. *Nature Geoscience*, *2*(1), 67–72. https://doi.org/10.1038/ngeo382

van Sebille, E., Griffies, S. M., Abernathey, R., Adams, T. P., Berloff, P., Biastoch, A., et al. (2018). Lagrangian ocean analysis: Fundamentals and practices. *Ocean Modelling*, *121*, 49–75. https://doi.org/10.1016/j.ocemod.2017.11.008

van Sebille, E., Spence, P., Mazloff, M. R., England, M. H., Rintoul, S. R., & Saenko, O. A. (2013). Abyssal connections of Antarctic Bottom Water in a Southern Ocean State Estimate. *Geophysical Research Letters*, *40*(10), 2177–2182. https://doi.org/10.1002/grl.50483

Ypma, S., Brüggemann, N., Georgiou, S., Spence, P., Dijkstra, H., Pietrzak, J., & Katsman, C. (2019). Pathways and watermass transformation of Atlantic Water entering the Nordic Seas through Denmark Strait in two high resolution ocean models. *Deep Sea Research Part I: Oceanographic Research Papers*, *145*, 59–72. https://doi.org/10.1016/j.dsr.2019.02.002

Zou, S., & Lozier, M. S. (2016). Breaking the linkage between Labrador Sea water production and its advective export to the subtropical gyre. *Journal of Physical Oceanography*, *46*(7), 2169–2182. https://doi.org/10.1175/JPO-D-15-0210.1

Zou, S., Lozier, M. S., Li, F., Abernathey, R., & Jackson, L. (2020). Density-compensated overturning in the Labrador Sea. *Nature Geoscience*, *13*(2), 121–126. https://doi.org/10.1038/s41561-019-0517-1